This is an author-created, un-copyedited version of an article published inEngineering Structures. The version of record is available online at https://doi.org/10.1016/j.engstruct.2019.03.032 ©2019 Elsevier.

Cam-based passive variable friction device for structural control

Austin Downey[a], Connor Theisen[b], Heather Murphy[c], Nicholas Anastasi[c], Simon Laflamme[d,e]

[a]*Department of Mechanical Engineering, University of South Carolina, Columbia, SC 29208, USA*
[b]*Department of Industrial and Manufacturing Systems Engineering, Iowa State University, Ames, IA 50011, USA*
[c]*Department of Mechanical Engineering, Iowa State University, Ames, IA 50011, USA*
[d]*Department of Civil, Construction, and Environmental Engineering, Iowa State University, Ames, IA 50011, USA*
[e]*Department of Electrical and Computer Engineering, Iowa State University, Ames, IA 50011, USA*

Abstract

A solution to increasing the resiliency of civil structures with respect to natural and man-made hazards is the implementation of supplemental damping systems. These systems can be constructed using passive, active, and semi-active devices. In particular, passive devices are widely accepted in the field of structural engineering, because they do not require power to operate and can be holistically integrated into the structural design process. This paper investigates the use of 3D printing technology to expand on the possibilities in passive damping, notably in the fabrication of a variable friction device. This device uses a 3D printed cam with a pre-defined surface profile to vary the normal forces applied to a traditional sliding plate friction system. It follows that these varying forces develop a variable damping force that is dependent on the device's displacement. In this work, a friction model is developed to characterize the device's behavior. This model is then validated on various cam profiles by exposing the device to a set of harmonic motions and to a nonstationary motion. Results show a high level of agreement between the experimental results and analytical model.

Keywords: variable friction, passive device, structural control, vibration mitigation, supplemental damping, displacement control, 3D printing
2018 MSC: 00-01, 99-00

1. Introduction

Motion-based design engineering is a method that consists of designing a structural system to limit structural motion to a prescribed level of performance. This design methodology can yield lighter and more efficient structural systems, therefore, resulting in important economic benefits. The design of a structural system for motion is typically conducted by appropriately sizing stiffness elements and supplemental damping systems for a given hazard type and magnitude. Supplemental damping plays an important role in vibration mitigation by absorbing energy input to the system, but must include damping mechanisms in the form of passive, active, or semi-active devices [1]. Passive mechanisms, and increasingly semi-active devices, have gained popularity and are now widely accepted by the field of structural engineering [2, 3]. Various types of damping systems have been proposed, including tuned mass/liquid dampers [4, 5, 6], viscoelastic fluid dampers [7, 8, 9], base-isolation systems [10, 11, 12], and friction dampers.

Friction damping systems are of particular interest, because of their typical low acquisition and maintenance cost, easy installation, and high mitigation limits [3, 13]. Additionally, friction dampers can operate over a greater bandwidth than other

*Corresponding author
Email address: austindowney@sc.edu (Austin Downey)

damping systems as they do not need to be tuned to specific excitation frequencies. Various passive friction systems can be found in the literature. Aiken et al. [14, 15] tested the Sumitomo Friction Damper developed by Sumitomo Metal Industries, Ltd., Japan. This damper is a cylinder device with friction material that slides on the inner surface of the steel tubing. While similar to a viscoelastic fluid damper in that both devices are designed to dissipate energy through linear stroke, this friction damper benefits from reduced maintenance cost as no oil retaining seals need to be inspected. Others have investigated the damping capabilities of connections with added friction material. For example, Pall et al. [16] proposed a slotted bolt connection at a typical beam-brace connection in a steel frame. Morgen et al. [17] studied a similar slotted joint system but adopted the concept for use at the beam-to-column connection in post-tensioned precast concrete. These solutions, while functional and easy to implement, do not offer any ability to vary their damping forces.

A solution is to vary the friction force through a semi-active mechanism. Various semi-active friction mechanisms and configurations have been proposed. Lu et al. [18] developed a semi-active damper that used a leverage mechanism along with a movable central pivot to control the damping force generated by a traditional passive friction damper. The damper was demonstrated both numerically and experimentally using several different ground motions and demonstrated a maximum damping force of 0.1 kN. Pardo-Varela et al. [19] proposed and studied a semi-active friction damper were piezoelectric actuators act on the device's clamping system to provide a variable normal force. Experimental results demonstrated that the device could obtain damping forces up to 23 kN. In addition to these devices, various automotive and industrial braking mechanisms have been explored for use in the control of structures. Samani et al. [20] adapted an automotive disk caliper and experimentally demonstrated that the damper was capable of developing damping forces ranging from 8 to 20 kN. Cao et al. [21] developed a semi-active damper that utilized a dual servo drum brake, similar to those found on semi-trailers, and was capable of developing 2.2 kN of damping force but suffered from a high amount of backlash caused by the rotation of the brake shoes. Downey et al. [22] developed a damper based on an industrial band brake, typically found in mining or ship mooring applications, that was capable of developing 45 kN of damping force while only needing a 0.27 kN of input force. These devices, while capable of altering their damping characteristics and providing performance over a wide frequency bandwidth, require power input and control algorithms to function properly.

In recent years, some researchers have investigated passive variable friction dampers (PVFDs) where the damping force varies as a function of displacement. Panchal et al. [12] developed a base isolation system that consisted of a concave surface with variable surface friction coefficients. The concept of altering the damping forces through variations in the coefficient of friction was recently studied by [23], where a generalized response was developed for such systems along with a design approach. Closer to the context of this study, Wang et al. [24] developed a displacement-dependent passive friction damper termed the arc-surfaced frictional damper. Unlike the previous base isolation system, variable friction is provided through the device's geometry. The damper was capable of generating an increase in damping force when displaced. Experimental results showed that a maximum damping force of 12 kN could be achieved with the current apparatus. Amjadian et al. [25] proposed a device that used both a friction and eddy current mechanism in parallel to generate a passive damper whose damping force decreases with an increase in displacement.

The development of customizable passive variable friction systems could be beneficial in structural control, as one could design the hysteretic loop to provide crafted mitigation capabilities within a motion-based design approach. The objective of this paper is to introduce a novel PVFD enabling easily customizable frictional behaviors. The device is a cam-based displacement dependent passive friction damper that is capable of varying its damping force as a function of displacement. This variation in damping force is obtained through the selection of a cam profile. Another benefit of the proposed cam-based damping device is that only the cams need to be replaced to alter the damping characteristics of the damping device, therefore allowing for a single damping device frame to host a diverse set of cam profiles. This feature could help in reducing the development and manufacturing cots in structures where a large number of dampers with different damping characteristics are needed. While the fabrication of a large amount of custom cam profiles requiring specific geometries could be expensive to

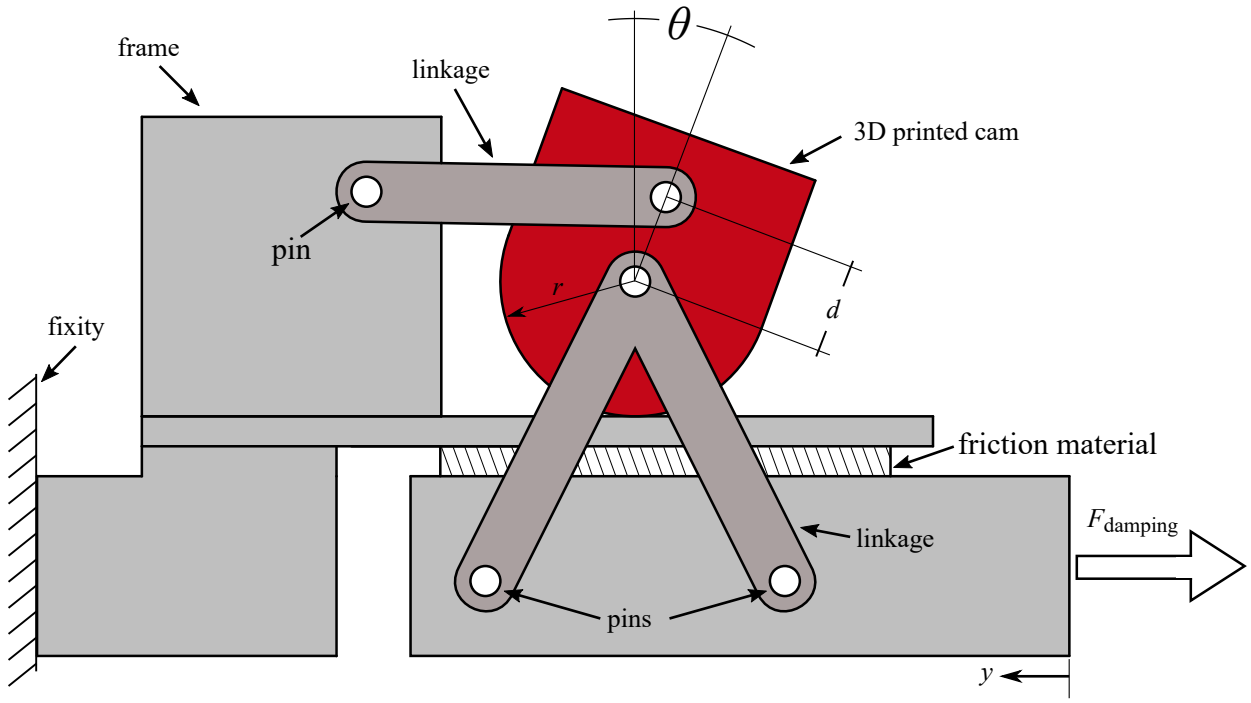

Figure 1: Schematic representation of the proposed cam-based displacement dependent passive variable friction device.

produce using existing manufacturing methods, a solution of interest lies in the use of additive manufacturing to enable PVFD technology. Additive manufacturing, such as 3D printing, rapid prototyping, and direct digital manufacturing, is of growing interest to the structural community [26] and its use in the development of complex cam shapes for this cam-based damper may help to greatly reduce the costs associated with manufacturing [27]. In this paper, the cam-based displacement dependent passive variable friction device is presented and an analytical model for the cams damping force is introduced. The model is experimentally validated on various 3D printed prototypes.

2. Proposed PVFD

The proposed PVFD is a cam-based displacement controlled damper that can generate a range of hysteresis behaviors, dependent on the cam selected for the device. It consists of a traditional sliding friction plate-based damper in combination with a displacement controlled cam that is used to generate the normal force applied to the friction material. A schematic of the device is shown in Figure 1 where the red cam is interchangeable and can be customized to produce a variety of damping characteristics. Due to the damper's passive nature, it is capable of near instantaneous reactions to lateral displacements, y. This feature is particularly useful for environments where the forces applied to the damper are unpredictable and instantaneous (e.g. blast loadings), because the magnitude of damping is dependent on the amplitude of the lateral displacement.

2.1. Implementation into a structural system

The proposed PVFD is designed to dissipate lateral displacements via friction. The device can be installed into configurations in which it can leverage such lateral displacements. The PVFD is capable of generating damping in a variety of installation configurations due to the rigidity of the system. In particular, the PVFD is well suited for nearly any damper configuration currently using viscous fluid dampers because both damper types are designed to dissipate energy through linear strokes. Two possible configurations are illustrated in Figure 2. The

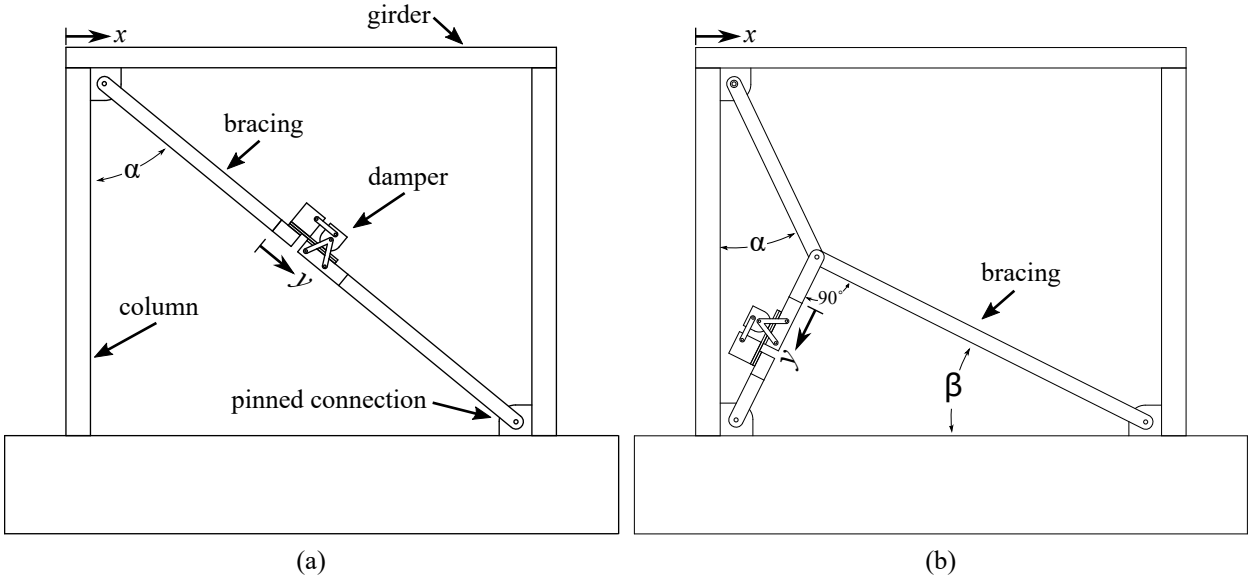

Figure 2: Two possible configurations for the friction device installed within a building's lateral load resisting system: (a) diagonal strut; (b) toggle configuration.

first, shown in Figure 2(a), positions the PVFD in a diagonal strut of a frame. The device is activated by movement in the frame's lateral direction x, where y is the lateral displacement in the device's frame of reference as shown in Figure 1. For the implementation shown in Figure 2(a), the displacement of the device can be expressed as:

$$y = \frac{x}{\cos(\alpha)} \tag{1}$$

Additionally, Figure 2(b) depicts the PVFD in a toggle brace configuration [28]. The toggle brace is used in structural motion engineering to increase the displacement of the damping devices, allowing them to be more effective in applications of small structural drift [29]. Here, the device is positioned on the short strut in a toggle configuration and the displacement at the device can be expressed as:

$$y = x \cdot \frac{\sin(\alpha)}{\cos(\alpha + \beta)} \tag{2}$$

Other potential insulation configurations include a chevron, scissors-jack [30], or other forms of the previously discussed toggle brace [29].

2.2. Friction mechanism

The PVFD is modeled by considering the friction interfaces to provide a direct physic-based characterization. Other hysteresis modeling approaches have been applied for the modeling of friction dampers (e.g. Bouc-Wen model [31]), but are not considered in this preliminary work. The varying damping force of the device is produced through the varying normal force applied to the friction material. This normal force is developed as a function of the cam's geometry in addition to the preloading force applied to the cam. The geometry of the cam's contact surface can be defined by modifying the general equation of an ellipse in polar notation:

$$r(\theta) = \frac{a \cdot b}{\sqrt{a^2 \sin^2\left(\theta - \frac{\pi}{2}\right) + \mathrm{b}^2 \cos^2\left(\theta - \frac{\pi}{2}\right)}} \tag{3}$$

where $r(\theta)$ is the radius of the cam that is acting to compress the friction material and is a function of the cam's rotation, θ. Here, r is measured from the origin of the polar coordinate system located at the center of the cam's lower hole as annotated in Figure 1. The $\frac{\pi}{2}$ term in Equation 3 is used to allow for θ to be measured from the vertical position of a centered cam, as shown in Figure 1. The parameters a and b are the semi-major and semi-minor axes of the ellipse, respectively, and are used in determining the cam profiles as detailed in Figure 3(a). Therefore, when the cam is centered ($\theta = 0$) the radius of the cam action on the friction material is equal to b. The rotation of the cam, θ can be

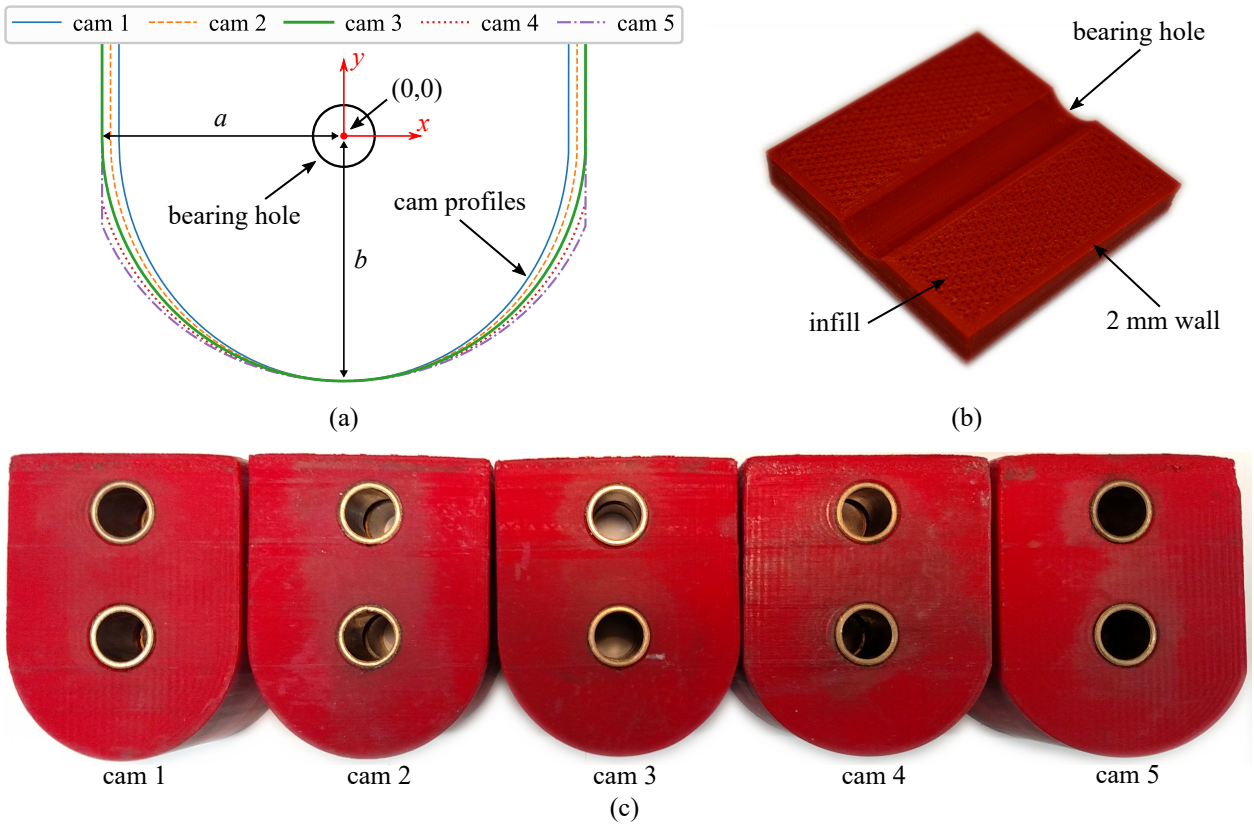

Figure 3: The construction of the cams showing the: (a) five cam profiles; (b) a cross-section of a partially completed cam; and (c) five cams of varying geometries considered in this study.

expressed in terms of displacement at the device, y:

$$\theta = \tan^{-1}\left(\frac{y}{d}\right) \tag{4}$$

where d is the distance between the two holes of the cam as annotated in Figure 1. Next, a change in radius as a function of cam rotation, $\Delta r(\theta)$, can be determined by developing a cam with a circular profile about the origin (i.e. $a = b = r$). The radius of this circle cam, r_{circle} is independent of θ as the radius is constant for any given rotation of the cam. Therefore, $\Delta r(\theta)$ can be calculated as $\Delta r(\theta) = r(\theta) - r_{\text{circle}}$ and the change in normal force for a cam profile that varies from that of a circle cam profile will be :

$$F_{\text{N,cam}}(\theta) = K\Delta r(\theta) \tag{5}$$

where, ($F_{\text{N,cam}}$) is the normal force developed by the cam, K is the stiffness of the device in the orientation of the normal force. Stiffness K is affected by various components within the device including the 3D printed cam, metal linkages, synthetic friction material, and the geometry of the cantilevered aluminum plate. The force ($F_{\text{N,cam}}$) needs to be added to the preloading force $F_{\text{N,preload}}$, which is utilized to apply a constant nominal normal force to the friction material. The preload force $F_{\text{N,preload}}$ is independent of θ and is quantified as the total compressive force on the cam when θ=0. In particular, $F_{\text{N,preload}}$ sets the nominal damping capacity of the device while the cam geometry is used to adjust the capacity as a function of the lateral displacement y. The total normal force acting on the friction material is given by:

$$F_{\text{N}}(\theta) = F_{\text{N,preload}} + F_{\text{N,cam}}(\theta) \tag{6}$$

It follows that the Coulomb friction model can be used to estimate the kinetic damping force (F_{kinetic}) for any given rotation of the cam when the coefficient of kinetic friction (μ) for the friction material is known. Therefore, $F_{\text{kinetic}}(\theta)$ is given as:

$$F_{\text{kinetic}}(\theta) = \mu F_{\text{N}}(\theta) \tag{7}$$

The LuGre friction model [32] is used to capture the dynamic properties of the sliding friction interface. It is an integrated dynamic friction model derived from the elasticity at the contact surface of two sliding surfaces. The model assumes that the friction material is constituted of an infinite number of bristles that deform elastically when one surface moves over the other surface. The LuGre model is capable of reproducing the stick-slip motion and Stribeck effect [33, 34] and has been applied to a wide range of friction systems due to its simple formulation, and effectiveness [35, 36, 37]. First, the static friction force (F_{static}) is taken by scaling the kinetic (F_{kinetic}) force by 0.98. Thereafter, the device's damping force (F_{damping}) is computed using the LuGre model's governing equation:

$$F_{\text{damping}} = \sigma_0 z + \sigma_1 \dot{z} + \sigma_2 \dot{y} \tag{8}$$

where σ_0 describes the spring-like (stiffness) behavior at the contact point of the assumed bristle for small displacements, σ_0 is termed the aggregate bristle stiffness and has units of $\text{N}\cdot\text{m}^{-1}$, σ_1 is the damping coefficient that represent the damping associated with the presliding displacement (also termed micro-displacement) and is expressed in $\text{N}\cdot\text{s}\cdot\text{m}^{-1}$, and σ_2 is a memoryless, velocity-dependent term for the kinetic friction component of the predicted friction force F_{damping} and is also expressed in the units $\text{N}\cdot\text{m}^{-1}$. The LuGre model parameter (σ_0, σ_1 and σ_2) are experimentally determined. The state variable, z, is an evolutionary variable that represents the elastic deformation of the bristle and can be interpreted as the average bristle deflection between the two sliding surfaces and allows the LuGre function to account for reversal of the sliding interfaces. It is obtained by solving the first order differential equation:

$$\dot{z} = \dot{y} - \sigma_0 \frac{|\dot{y}|}{g(\dot{y})} z \tag{9}$$

where $g(\dot{y})$ models the Stribeck effect, is a function of the sliding velocity, and can be written:

$$g(\dot{y}) = F_{\text{kinetic}} + (F_{\text{static}} - F_{\text{kinetic}}) \exp(-(\dot{y}/\dot{y}_s)^2) \tag{10}$$

where $\dot{y}_s$ is a constant representing the Stribeck velocity and is expressed in m/s. For a more detailed investigation of the LuGre model, the interested reader is referred to [33]. In this work, the solution to the ordinary differential equation was obtained numerically using the SciPy package for python [38].

Table 1: Design parameters for the cams used in this study.

	cam				
parameters	1	2	3	4	5
a (mm)	29.3	30.4	31.5	32.6	33.7
b (mm)	31.5	31.5	31.5	31.5	31.5
w (mm)	58.6	60.8	63.0	63.0	63.0

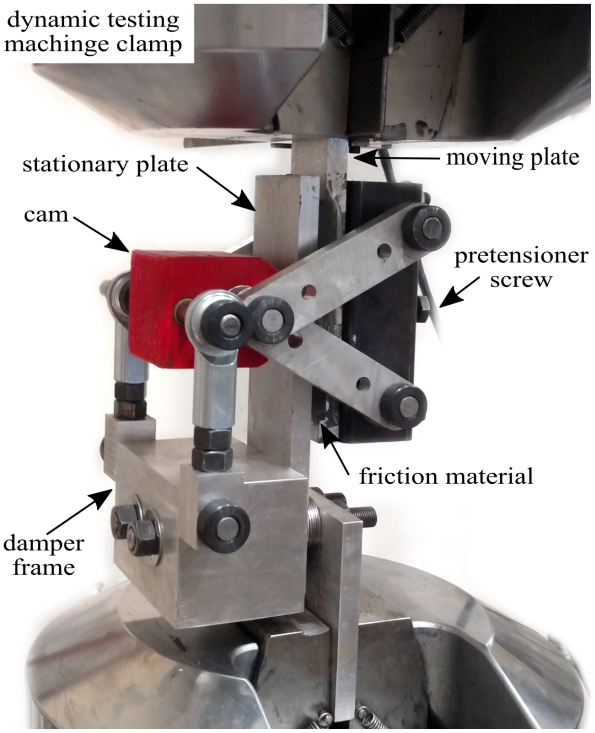

Figure 4: Experimental test setup with the key components annotated.

3. Experimental Validation

In this section, the prototype apparatus and the testing mechanisms used in the experimental validation of the displacement-dependent PVFD are described.

3.1. Prototypes

The cams developed for this study are detailed in Figure 3 while a prototype version of the proposed damping device is shown in Figure 4. Video 1 presents the device under test with cam 5 installed. The profile of these cams are defined by the parameters listed in Table 1 used with Equation 3. For this study, cam 3 is a cam whose contact surface is defined by a circle ($a = b$). The hysteresis behavior associated with this cam is similar to that

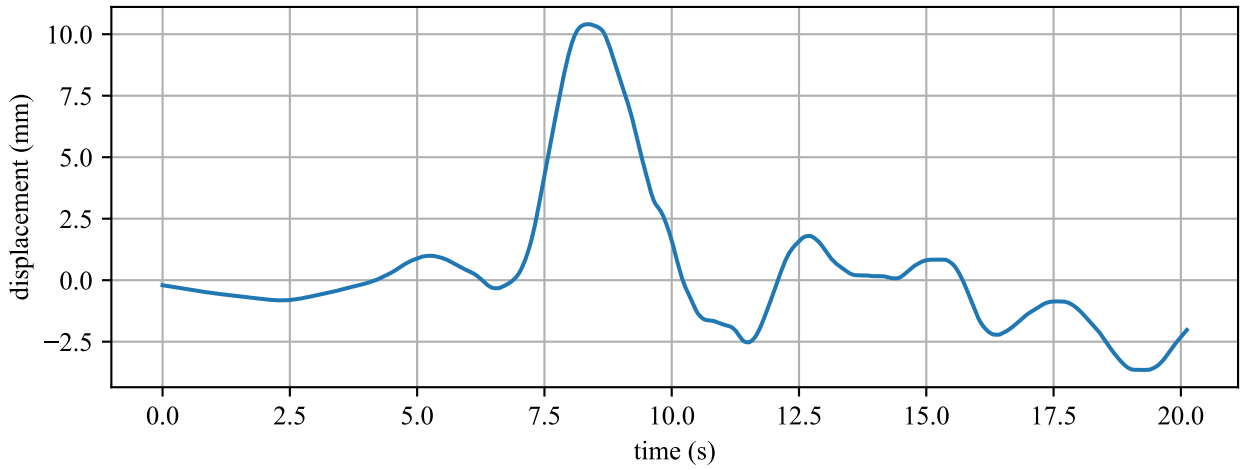

Figure 5: Displacement-controlled loading developed from the acceleration data recorded during the 1989 Loma Prieta earthquake [39].

found in a traditional passive friction damper [15]. In comparison, the contact surfaces of cams 1 and 2 are defined by ellipses with a semi-major axis less than that defined by the circle and therefore decrease the damping force when the friction plates are displaced from the origin. This hysteresis behavior for cams 1 and 2 is similar to that generated by the passive electromagnetic eddy current friction damper developed by Amjadian et al. [25]. Conversely, cams 4 and 5 are defined by ellipses with a semi-major axis beyond that defined by a circle and increase the damping force when the device is displaced from its origin. The characteristic of the hysteresis behavior developed by these two cams resembles the hysteresis behavior of the arc-surfaced frictional damper proposed by Wang et al. [24]. The outline of the 3D printed cam profiles are presented in Figure 3(a). The cams in this study were fabricated from acrylonitrile butadiene styrene (ABS) plastic using an extrusion-type 3D printer with a 2 mm wall thickness and a 75% triangle-type pattern infill. A cross-section of a cam is shown in Figure 3(b). After cleaning up the bearing holes, plain bronze bushings were press fit into the holes and reamed to the size of the shaft. The layer-by-layer approach of extrusion-type 3D printers leaves an uneven surface on the contact surface of the cam, which necessitated light sanding using a 220 grit emery cloth. Lastly, a light layer of Polytetrafluoroethylene (PTFE) (also known as Teflon®) multipurpose aerosol lubricant was applied to the contact surface of the cam and wiped down to ensure that a minimal and consistent layer remained. The width w of each cam is equal to twice the semi-major axis ($2a$), giving 58.6 mm and 60.8 mm for cams 1 and 2, respectively, and 63.0 mm for the other cams. The five cams prototyped for this study are presented in Figure 3(c).

Table 2: LuGre model parameters used in this study.

σ_0 (N·m^{-1})	σ_1 (N·s·m^{-1})	σ_2 (N·s·m^{-1})	$\dot{y}_s$ (m/s)
2.605×10^6	826	1049	0.001

The prototype device used in this study was designed to verify the concept of using interchangeable cams to control damping forces. As such, the prototyping task was conducted focusing on simple cam designs rather than on the design of the damping force itself. Also, obtaining higher damping forces would require the construction of a more rigid device and the use of a stiffer material for the cams. In addition to obtaining higher damping forces, future device designs would need to consider the high-speed velocity dependency, long-term durability of friction material, and the lateral stiffness of the device. However, these considerations are out-of-scope of this introductory study. In this work, an aluminum test device was constructed for holding the cams and the friction material. Plain bronze bushings or steel spherical rod ends were used, along with a ground steel shaft,

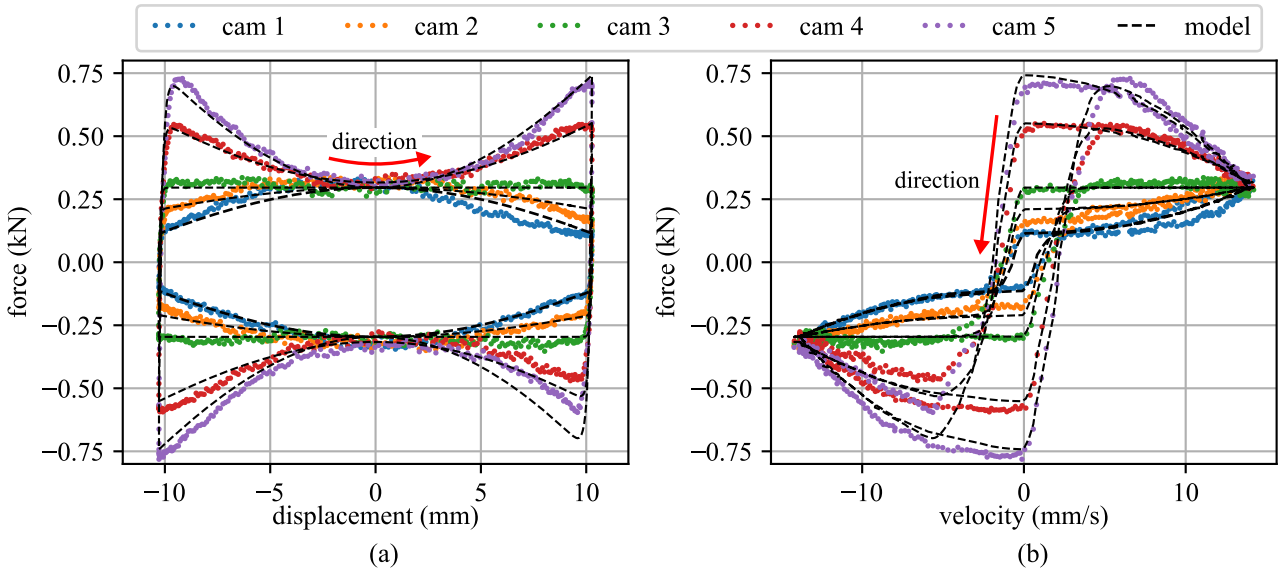

Figure 6: Experimental test results for cams 1 - 5, tested at 0.2 Hz showing the: (a) force-displacement loops; (b) force-velocity loops.

for all of the connection points to greatly reduce the backlash in the system. The backlash phenomenon is found in reversible devices and manifests itself as a significant reduction in forces upon reversal [21, 22, 24, 40]. A block and a pretensioner screw were mounted on the underside of the damper (right-hand side in Figure 4) for applying the pretension force, $F_{\mathrm{N,preload}}$, required for the damper to function.

The friction material used in this test was a flexible, metal free, asbestos free, elastomer-resin bonded friction material designed for use as friction material in industrial brakes and clutches [41]. A friction dynamic coefficient of 0.4, obtained from the materials data sheet, was used in this work. The sample measured $9.5 \times 63 \times 120$ mm^2 and was attached to the aluminum plate using a two-part industrial epoxy (JB-Weld®). A preload force of 0.7 kN was applied using the pretensioner screw as annotated in Figure 4. The total stiffness of the device in the orientation of the normal force, K, was determined from the experimental data for each cam by calculating the stiffness of the device when the device is at its maximum positive displacement before the rotation was reversed. The points from which the device's stiffness for each cam was calculated are the upper right-hand corners of the hysteresis curves in figure 6(a). The value of K was found to vary depending on whether the cam was being relaxed (i.e. cams 1 and 2) or compressed (i.e. cams 4 and 5) with a change in displacement. During this study, a K value of 1900 kN/m was used for cams 1 and 2 while a value of 5100 kN/m was used for cams 4 and 5. The K value associated with cam 3 is irrelevant as its damping is set solely by the preload force ($F_{\mathrm{N,cam}} = 0$ in Equation 6) and is therefore not dependent on the stiffness of the cam. Variations in the devices stiffness can be attributed to: cams 1 and 2 having a smaller width than cams 4 and 5, a slight asymmetry in the linkage that connects the cam to the moving plate, deflection of the cantilever plate that transfers the normal force to the friction material, a function of the 75% infill used in the ABS plastic, and/or relaxation properties of the friction material. This question is left to future work.

3.2. Methodology

Characterization of the prototype device was performed in a servo-hydraulic testing machine with an integrated load cell mounted to the top clamp and used to acquire the damping forces developed by the damper. Each cam was subjected to the same set of displacement-controlled harmonic excitations of 20 mm amplitude at five different frequencies: 0.05, 0.1, 0.2, 0.3, and 0.4 Hz. In addition to these harmonic excitations, the nonlinear response of the damper was tested using the nonstationary loading

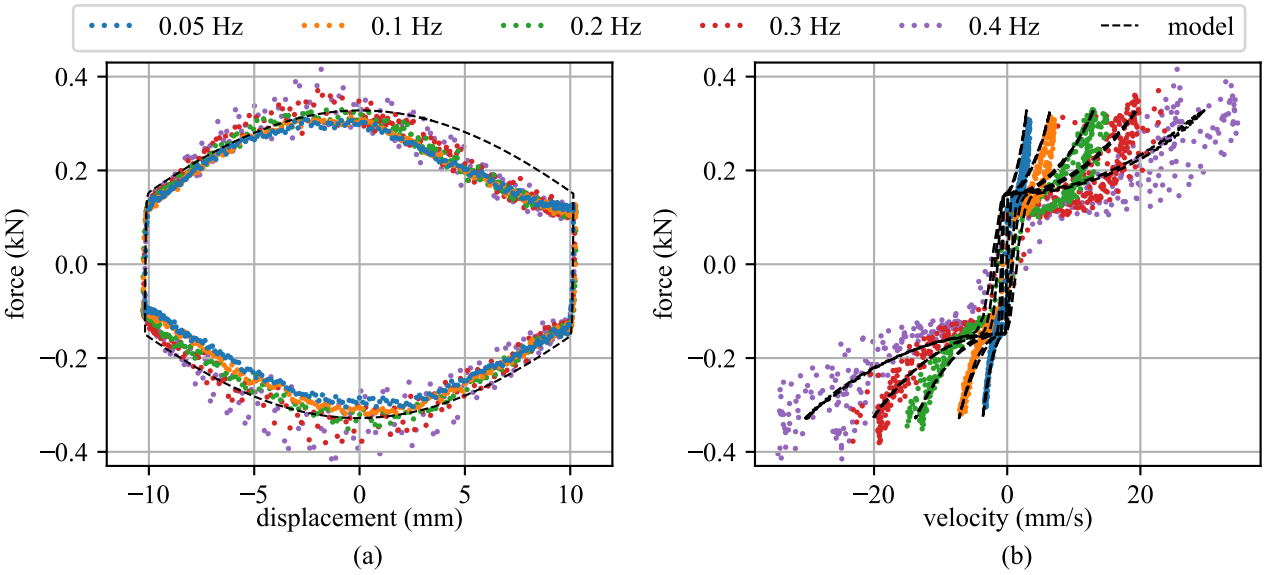

Figure 7: Experimental test results for cam 1 tested under the five frequencies considered in this study, showing the: (a) force-displacement loops; (b) force-velocity loops.

plotted in Figure 5. This displacement-controlled loading was developed from the acceleration data recorded during the 1989 Loma Prieta earthquake [39]. The purpose of this investigation is to validate the model using a complex time history rather than characterizing the prototype. The ground displacements were computed by double integrating the ground acceleration, with the building acting as a low-pass filter to remove the high-frequency components, and scaled to the device's maximum displacement of ±10 mm.

The LuGre friction model parameters were experimentally determined using the experimental data from the circle cam (cam 3) at an excitation frequency of 0.2 Hz. This cam was chosen as it produces a generally rectangular hysteresis loop, as shown in figure 6. Particle swarm optimization [42] was used to select the optimal values for the model parameters. Model parameters were solved for by minimizing the error between the experimental data and predicted damping force generated by the LuGre model. The LuGre model parameters obtained for cam 3 were found to be effective for all five cam profiles studied in this work and are used for every cam profile. The parameters used in this study are presented in table 2.

4. Results

The various damping forces generated by the device for the five cams understudy for the 0.2 Hz harmonic load are presented in Figure 6. Results are typical for all frequencies. The 0.2 Hz frequency was selected for illustration because it is in the middle of the five frequencies tested. The results demonstrate that the damping response of the proposed damping device can be altered through the selection of a cam profile. Overall, the simple LuGre friction model used in this study was shown to accurately predict the force generated by each cam, once the stiffness values have been estimated. A shortcoming of the friction model can be observed in cam's 4 and 5 whereupon reversal of the dampers direction of travel the model overshoots the damping force developed by the cams due to a slight asymmetry in the damping force generated by these cams. The asymmetry in the LuGre friction model is a function of the reversal of the sliding directions of the friction interfaces. The red arrows in Figure 6 denote the direction of the moving plate in terms of the hysteresis loop. For example, cam 5's hysteresis loop exhibits a rounded corner after the friction interface reverses its direction and starts to build up the friction force (top-left in Figure 6(a)). In comparison, a sharp corner is observable by the hysteresis loop when the friction interface reverses its direction (top-right in

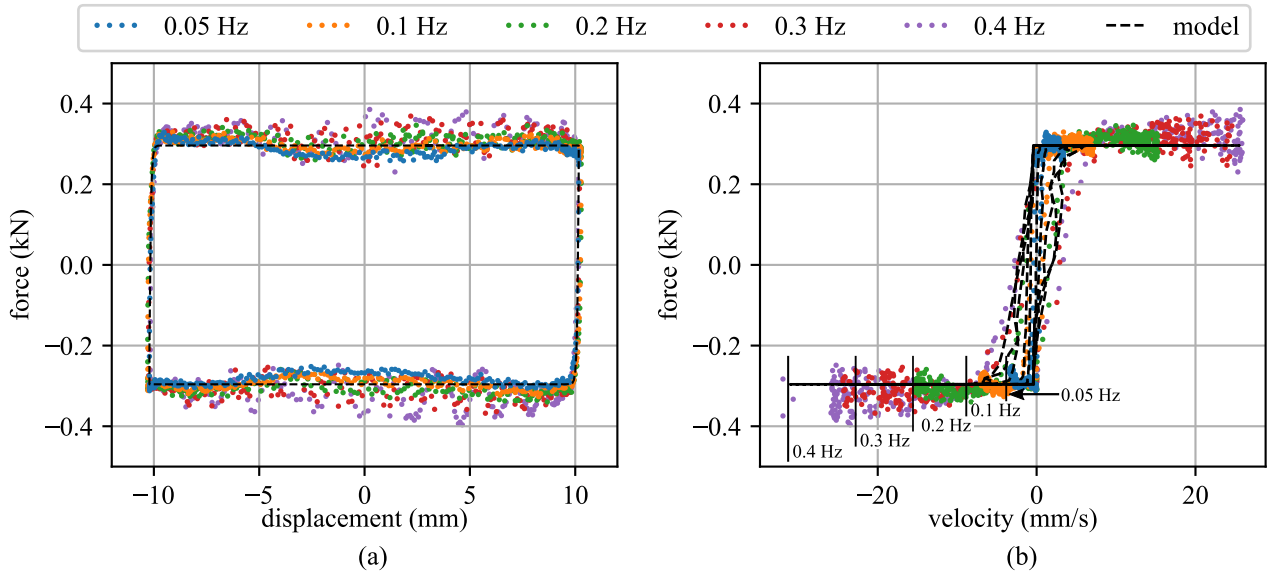

Figure 8: Experimental test results for cam 3 tested under the five frequencies considered in this study, showing the: (a) force-displacement loops; (b) force-velocity loops.

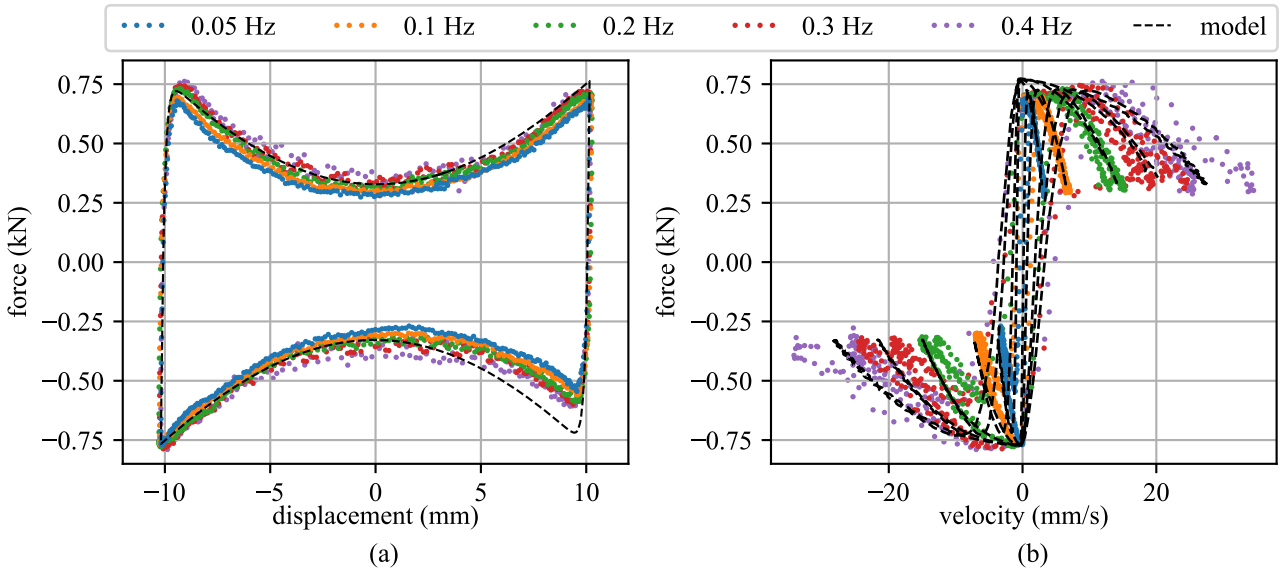

Figure 9: Experimental test results for cam 5 tested under the five frequencies considered in this study, showing the: (a) force-displacement loops; (b) force-velocity loops.

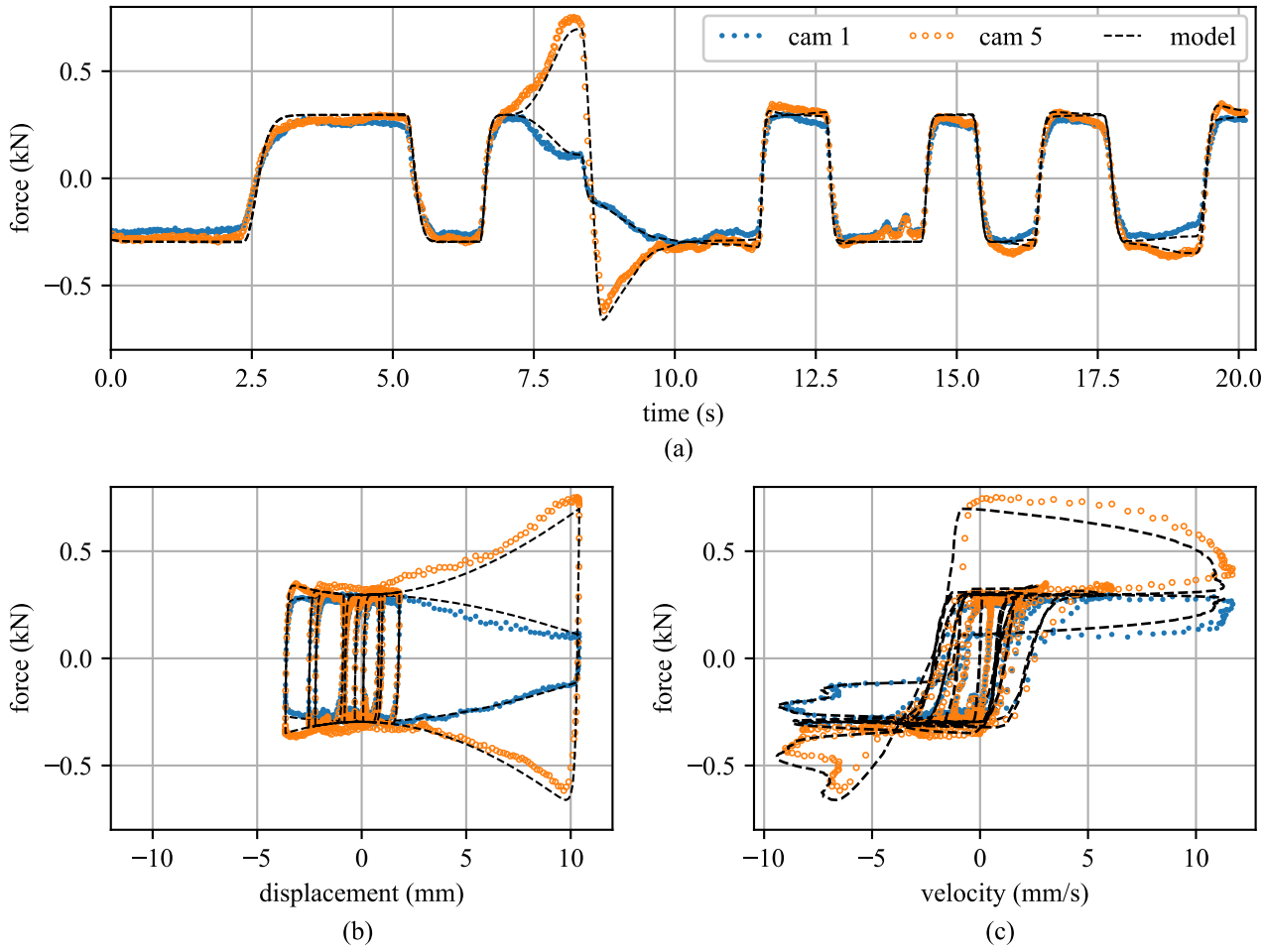

Figure 10: Experimental test results for cam 1 and cam 5 using the times-series displacement-controlled input derived from the 1989 Loma Prieta earthquake showing the: (a) time-series results; (b) force-displacement loop; (c) force-velocity loop.

Figure 6(a)) before building up a damping force in the opposite direction. Overall, the LuGre model is capable of accurately predicting damping forces generated by the damper, including the asymmetry introduced by the reversal of the friction interfaces.

The frequency dependence can be investigated from Figures 7 - 9, which plot the responses from cams 1, 3, and 5 for the five different frequencies tested. Cams 1 and 5 represent the two hysteresis behaviors with the highest potential interest, as demonstrated by the hysteresis developed by other PVFDs found in the literature [24, 25]. Cam 3 is shown because it produces the hysteresis behavior associated with a traditional passive friction damper [15]. Results for cam 3, presented in Figure 8, demonstrate the device experiences very little backlash during testing and that its force-displacement loop is similar to that of a passive friction damper, as expected. Cams 2 and 4 exhibited frequency dependent traits similar to the cams presented here, but are not shown for brevity. Overall, results demonstrate that the damping force can be taken as independent of the frequency applied to the system. Nevertheless, a small increase in damping force can be observed at the higher frequencies, but this is relatively small when compared to the overall damping forces generated by the device. At higher frequencies, the damping device did exhibit a higher level of noise in the damping force. This higher level of noise is clearly visible in the 0.4 Hz data presented in Figures 7(b) and 9(b). This noise is attributed to vibrations generated by the chattering of the dynamic testing machine.

The validation of the model is conducted on

Table 3: RMSE between the experimental and LuGre estimated force.

	RMSE (kN)				
	cam 1	cam 2	cam 3	cam 4	cam 5
0.05 Hz	46.7	29.5	21.5	50.1	97.3
0.1 Hz	42.5	25.3	17.5	40.7	79.2
0.2 Hz	39.5	31.4	26.1	39.3	64.3
0.3 Hz	39.9	38.6	34.4	42.8	58.4
0.4 Hz	46.5	51.5	50.1	73.2	91.5
Loma Prieta	73.8	51.0	49.9	54.7	55.8

the nonstationary loading derived from the 1989 Loma Prieta earthquake. Figure 10 are plots of the experimental results compared with the fit from the model for the force-time (Figure 10(a)), force-displacement (Figure 10(b)), and force-velocity (Figure 10(c)) relationships. For clarity, results are only shown for cams 1 and 5. Two models are shown in Figure 10, one for each cam. When the displacement is relatively small, these two cams develop similar damping values and therefore, similar model results. However, when the displacement present in the devices increases, for example at approximately 8 and 19 seconds, the damping force generated by the cams greatly contrast each other. The model demonstrates an excellent capability of predicting the proposed PVFD's damping force for the cams of interest. Lastly, disagreements between experimental and modeled force data were quantified using the root-mean-square error (RMSE) calculated in the time domain for each test. Results are tabulated in table 3

5. Summary and Conclusions

This paper presented a novel displacement-dependent passive variable friction damper intended for structural control applications. The damping force generated as a function of displacement is controlled by the selection of a specific cam profile. These cam profiles can be optimized for any number of varying design considerations that require specialized hysteresis loops. Furthermore, various categories of loadings in addition to multi-hazard events can be considered through a motion-based design procedure. To alleviate limitations in the fabrication of these custom devices using conventional manufacturing methods, the cams were 3D printed. These cams can be inserted, by design, into a common friction-plate-based apparatus, therefore reducing the cost of manufacturing and deployment of the system.

This work started by introducing an analytical model for the damping device based on the LuGre model for dry friction. Then, a prototype of the damping device was introduced and experimentally validated. The cams were 3D printed from ABS plastic with plain bronze bushings or steel spherical rod ends used for all the bearing surfaces. Five cams of different profiles were tested under five cyclic tests with varying frequencies for the purpose of characterizing the damping device. The prototypes were also exposed to a nonstationary load developed from a seismic excitation. Results demonstrated that the proposed model was capable of accurately predicting the damping force of the damper as a function of the displacement of the friction plates and the profile of the cam under consideration. Additionally, it was shown that the added damping force developed by the device is independent of the frequency of the applied excitation.

The validated prototype and friction model presented in this research advance the concept of 1) using displacement-dependent passive variable friction devices and 2) leveraging 3D printing technology for structural control, through presenting a damping device that is capable of delivering custom damping characteristics based on the selection of a cam profile. Avenues for future work include the development of more complex cam profiles optimized for various loading cases and studying the performance of the damping device within a structural system.

Acknowledgements

This material is based upon work supported by the National Science Foundation under Grants No. 1300960, 1463252, and 1537626. This work is also partly supported by the National Science Foundation Grant No. 1069283, which supports the activities of the Integrative Graduate Education and Research Traineeship (IGERT) in Wind Energy Science, Engineering and Policy (WESEP) at Iowa State University. Additional funding was provided by the Stewart Research Award through the Iowa State Foundation. The support of these agencies is gratefully acknowledged. Any opinions, findings, and conclusions or recommendations expressed in

this material are those of the authors and do not necessarily reflect the views of the National Science Foundation. The authors would also like to thank Wyman Martinek for help with experimental testing.

References

[1] J. Connor, S. Laflamme, Structural Motion Engineering, Springer International Publishing, 2014. doi:10.1007/978-3-319-06281-5.
URL https://doi.org/10.1007/978-3-319-06281-5

[2] M. Symans, F. Charney, A. Whittaker, M. Constantinou, C. Kircher, M. Johnson, R. McNamara, Energy dissipation systems for seismic applications: current practice and recent developments, Journal of structural engineering 134 (1) (2008) 3–21.

[3] T. E. Saaed, G. Nikolakopoulos, J.-E. Jonasson, H. Hedlund, A state-of-the-art review of structural control systems, Journal of Vibration and Control 21 (5) (2013) 919–937. doi:10.1177/1077546313478294.
URL https://doi.org/10.1177/1077546313478294

[4] M. J. Tait, N. Isyumov, A. A. E. Damatty, Performance of tuned liquid dampers, Journal of Engineering Mechanics 134 (5) (2008) 417–427. doi:10.1061/(asce)0733-9399(2008)134:5(417).
URL https://doi.org/10.1061/(asce)0733-9399(2008)134:5(417)

[5] F. Ubertini, I. Venanzi, G. Comanducci, Considerations on the implementation and modeling of an active mass driver with electric torsional servomotor, Mechanical Systems and Signal Processing 58-59 (2015) 53–69. doi:10.1016/j.ymssp.2014.12.010.
URL https://doi.org/10.1016/j.ymssp.2014.12.010

[6] M. G. Soto, H. Adeli, Tuned mass dampers, Archives of Computational Methods in Engineering 20 (4) (2013) 419–431. doi:10.1007/s11831-013-9091-7.
URL https://doi.org/10.1007/s11831-013-9091-7

[7] L.-Y. Lu, C.-C. Lin, G.-L. Lin, Experimental evaluation of supplemental viscous damping for a sliding isolation system under pulse-like base excitations, Journal of Sound and Vibration 332 (8) (2013) 1982–1999. doi:10.1016/j.jsv.2012.12.008.
URL https://doi.org/10.1016/j.jsv.2012.12.008

[8] S. Sorace, G. Terenzi, Seismic protection of frame structures by fluid viscous damped braces, Journal of Structural Engineering 134 (1) (2008) 45–55. doi:10.1061/(asce)0733-9445(2008)134:1(45).
URL https://doi.org/10.1061/(asce)0733-9445(2008)134:1(45)

[9] A. Q. Bhatti, Performance of viscoelastic dampers (VED) under various temperatures and application of magnetorheological dampers (MRD) for seismic control of structures, Mechanics of Time-Dependent Materials 17 (3) (2012) 275–284. doi:10.1007/s11043-012-9180-2.
URL https://doi.org/10.1007/s11043-012-9180-2

[10] R. Ibrahim, Recent advances in nonlinear passive vibration isolators, Journal of Sound and Vibration 314 (3-5) (2008) 371–452. doi:10.1016/j.jsv.2008.01.014.
URL https://doi.org/10.1016/j.jsv.2008.01.014

[11] E. Sato, S. Furukawa, A. Kakehi, M. Nakashima, Full-scale shaking table test for examination of safety and functionality of base-isolated medical facilities, Earthquake Engineering & Structural Dynamics 40 (13) (2011) 1435–1453. doi:10.1002/eqe.1097.
URL https://doi.org/10.1002/eqe.1097

[12] V. R. Panchal, R. S. Jangid, Variable friction pendulum system for near-fault ground motions, Structural Control and Health Monitoring 15 (4) (2008) 568–584. doi:10.1002/stc.216.
URL https://doi.org/10.1002/stc.216

[13] C. D. Johnson, Design of passive damping systems, Journal of Vibration and Acoustics 117 (B) (1995) 171. doi:10.1115/1.2838659.
URL https://doi.org/10.1115/1.2838659

[14] I. D. Aiken, J. M. Kelly, Earthquake simulator testing and analytical studies of two energy-absorbing systems for multistory structures, Ph.D. thesis, University of California, Berkeley (1990).

[15] I. D. Aiken, D. K. Nims, A. S. Whittaker, J. M. Kelly, Testing of passive energy dissipation systems, Earthquake Spectra 9 (3) (1993) 335–370. doi:10.1193/1.1585720.
URL https://doi.org/10.1193/1.1585720

[16] A. S. Pall, C. Marsh, Response of friction damped braced frames, Journal of Structural Engineering 108 (9) (1982) 1313–1323.
URL http://www.palldynamics.com/fr/pdf/40Pall_doc1.pdf

[17] B. Morgen, Y. Kurama, A friction damper for post-tensioned precast concrete beam-to-column joints, PCI J 49 (4) (2004) 112–133.

[18] Y. Liu, H. Matsuhisa, H. Utsuno, Semi-active vibration isolation system with variable stiffness and damping control, Journal of Sound and Vibration 313 (1-2) (2008) 16–28. doi:10.1016/j.jsv.2007.11.045.
URL https://doi.org/10.1016/j.jsv.2007.11.045

[19] J. Pardo-Varela, J. C. de la Llera, A semi-active piezoelectric friction damper, Earthquake Engineering & Structural Dynamics 44 (3) (2014) 333–354. doi:10.1002/eqe.2469.
URL https://doi.org/10.1002/eqe.2469

[20] H. R. Samani, M. Mirtaheri, A. P. Zandi, Experimental and numerical study of a new adjustable frictional damper, Journal of Constructional Steel Research 112 (2015) 354–362. doi:10.1016/j.jcsr.2015.05.019.
URL https://doi.org/10.1016/j.jcsr.2015.05.019

[21] L. Cao, A. Downey, S. Laflamme, D. Taylor, J. Ricles, Variable friction device for structural control based on duo-servo vehicle brake: Modeling and experimental validation, Journal of Sound and Vibration 348 (2015) 41–56. doi:10.1016/j.jsv.2015.03.011.
URL https://doi.org/10.1016%2Fj.jsv.2015.03.011

[22] A. Downey, L. Cao, S. Laflamme, D. Taylor, J. Ricles, High capacity variable friction damper based on band brake technology, Engineering Structures 113 (2016) 287–298. doi:10.1016/j.engstruct.2016.01.035.
URL https://doi.org/10.1016%2Fj.engstruct.2016.01.035

[23] S. Timsina, P. M. Calvi, Variable friction base isolation systems: Seismic performance and preliminary design, Journal of Earthquake Engineering (2018) 1–24doi:10.1080/13632469.2018.1504837.

[24] G. Wang, Y. Wang, J. Yuan, Y. Yang, D. Wang, Modeling and experimental investigation of a novel arc-surfaced frictional damper, Journal of Sound and Vibration 389 (2017) 89–100. doi:10.1016/j.jsv.2016.

11.019.
URL https://doi.org/10.1016/j.jsv.2016.11.019
[25] M. Amjadian, A. K. Agrawal, A passive electromagnetic eddy current friction damper (PEMECFD): Theoretical and analytical modeling, Structural Control and Health Monitoring 24 (10) (2017) e1978. doi:10.1002/stc.1978.
URL https://doi.org/10.1002/stc.1978
[26] M. Yossef, A. Chen, Applicability and limitations of 3d printing for civil structures, in: Proceedings of the 2015 Conference on Autonomous and Robotic Construction of Infrastructure, 2015, pp. 237–246.
URL https://lib.dr.iastate.edu/ccee_conf/35
[27] K. V. Wong, A. Hernandez, A review of additive manufacturing, ISRN Mechanical Engineering 2012 (2012) 1–10. doi:10.5402/2012/208760.
URL https://doi.org/10.5402/2012/208760
[28] D. P. Taylor, Toggle brace dampers: A new concept for structural control, in: Advanced Technology in Structural Engineering, American Society of Civil Engineers, 2000. doi:10.1061/40492(2000)10.
URL https://doi.org/10.1061/40492(2000)10
[29] M. C. Constantinou, P. Tsopelas, W. Hammel, A. N. Sigaher, Toggle-brace-damper seismic energy dissipation systems, Journal of Structural Engineering 127 (2) (2001) 105–112. doi:10.1061/(asce)0733-9445(2001)127:2(105).
URL https://doi.org/10.1061/(asce)0733-9445(2001)127:2(105)
[30] A. N. Sigaher, M. C. Constantinou, Scissor-jack-damper energy dissipation system, Earthquake Spectra 19 (1) (2003) 133–158. doi:10.1193/1.1540999.
URL https://doi.org/10.1193/1.1540999
[31] D.-W. Kang, S.-W. Jung, G.-H. Nho, J.-K. Ok, W.-S. Yoo, Application of bouc-wen model to frequency-dependent nonlinear hysteretic friction damper, Journal of Mechanical Science and Technology 24 (6) (2010) 1311–1317. doi:10.1007/s12206-010-0404-6.
[32] C. C. de Wit, H. Olsson, K. Astrom, P. Lischinsky, A new model for control of systems with friction, IEEE Transactions on Automatic Control 40 (3) (1995) 419–425. doi:10.1109/9.376053.
[33] K. Astrom, C. C. de Wit, Revisiting the LuGre friction model, IEEE Control Systems 28 (6) (2008) 101–114. doi:10.1109/mcs.2008.929425.
URL https://doi.org/10.1109/mcs.2008.929425
[34] H. Olsson, K. Åström, C. C. de Wit, M. Gäfvert, P. Lischinsky, Friction models and friction compensation, European Journal of Control 4 (3) (1998) 176–195. doi:10.1016/s0947-3580(98)70113-x.
URL https://doi.org/10.1016/s0947-3580(98)70113-x
[35] L. Freidovich, A. Robertsson, A. Shiriaev, R. Johansson, LuGre-model-based friction compensation, IEEE Transactions on Control Systems Technology 18 (1) (2010) 194–200. doi:10.1109/tcst.2008.2010501.
URL https://doi.org/10.1109/tcst.2008.2010501
[36] P. Lischinsky, C. C. de Wit, G. Morel, Friction compensation for an industrial hydraulic robot, IEEE Control Systems 19 (1) (1999) 25–32. doi:10.1109/37.745763.
URL https://doi.org/10.1109/37.745763
[37] T. Piatkowski, Dahl and LuGre dynamic friction models — the analysis of selected properties, Mechanism and Machine Theory 73 (2014) 91–100. doi:10.1016/j.mechmachtheory.2013.10.009.
URL https://doi.org/10.1016/j.mechmachtheory.2013.10.009
[38] E. Jones, T. Oliphant, P. Peterson, et al., Scipy: Open source scientific tools for Python (2001–).
URL http://www.scipy.org/
[39] PEER, Peer, pacific earthquake engineering research center (2010).
URL http://peer.berkeley.edu/peer_ground_motion_database
[40] S. Kannan, H. M. Uras, H. M. Aktan, Active control of building seismic response by energy dissipation, Earthquake Engineering & Structural Dynamics 24 (5) (1995) 747–759. doi:10.1002/eqe.4290240510.
URL https://doi.org/10.1002/eqe.4290240510
[41] B. R. E. G. . C. KG, data sheet: Bermskerl 5505, Brakenhof 7, 31629 Estorf, Post office box 1860, 31568 Nienburg, Germany (2007).
[42] L. J. V. Miranda, PySwarms: a research toolkit for particle swarm optimization in python, The Journal of Open Source Software 3 (21) (2018) 433. doi:10.21105/joss.00433.
URL https://doi.org/10.21105/joss.00433